ingegneria sismica
International Journal of Earthquake Engineering
Anno XLIII - Num. 3 - 2026

Study on the influence of carbide slag fly ash composite material on the compressive strength and corrosion resistance of low-carbon UHPC

Haozhe Pan[1,*] *and Xingpei Yan*[2]

[1] Faculty of Materials and Civil Engineering of Jiangsu University Jingjiang College, Zhenjiang 212028, Jiangsu, China

SUMMARY: *An improved deep neural network algorithm is proposed to predict the compressive strength and corrosion resistance of low-carbon ultra-high-performance concrete (UHPC) using carbide slag fly ash composite materials, and optimize the mix design. Firstly, 226 sets of sample datasets were collected from UHPC compressive strength and corrosion resistance test data, and preprocessed. Using principal component analysis weighting method to assign weights to input variables, randomly select some data as training and testing sets. Secondly, an improved deep neural network model is constructed by introducing weighted cross entropy loss to reduce class imbalance, and supervised contrastive learning is designed to enhance the model's feature extraction capability. Use Matlab software to train the model and analyze the prediction results. Empirical evaluations demonstrate that the optimized deep neural network architecture exhibits superior predictive performance and enhanced robustness when benchmarked against its predecessor. Specifically, the model achieves a 17.11% and 41.04% reduction in root mean square error (RMSE) values, coupled with corresponding decreases of 28.35% and 44.25% in mean absolute error (MAE) metrics. The proposed computational framework demonstrates exceptional predictive capacity for both mechanical (compressive strength) and durability (corrosion resistance) properties of ultra-high-performance concrete (UHPC) formulated with carbide slag-fly ash composites. This advancement enables data-driven optimization of mixture proportions tailored to specific strength requirements, thereby establishing a theoretical foundation for rational design of advanced cementitious composites.*

KEYWORDS: *Carbide slag fly ash; Ultra high-performance concrete; Compressive strength; Corrosion resistance; Mix proportion design; Deep neural network; Weighted cross entropy*

1 Introduction

Ultra-high-performance concrete (UHPC) represents an advanced class of cementitious composites characterized by exceptional mechanical properties, including elevated compressive strength, enhanced fracture toughness, and superior long-term durability under aggressive environmental conditions, which meets the development requirements of engineering light weighting, low carbonization, and assembly, and has broad prospects [1, 2]. However, traditional UHPC requires a large number of cementitious materials in the production process, which leads to high costs and limits its promotion and application. Adding carbide slag fly ash composite materials to UHPC can not only reduce the number of cementitious materials and production costs, but also reduce self-shrinkage, increase elastic modulus, compressive

*haozhepan89@163.com
https://doi.org/10.65102/is20261098
Published: 10 June, 2026

strength, and corrosion resistance [3, 4]. Given the escalating demand for infrastructure development in China, the integration of carbide slag-fly ash (CSFA) composite admixtures into ultra-high-performance concrete (UHPC) formulations represents an inevitable advancement in sustainable construction materials. Research focused on predictive modeling of mechanical (compressive strength) and durability (corrosion resistance) properties, along with optimized mixture design, is critical for advancing the practical application of CSFA-modified UHPC. While prior studies have made significant strides in UHPC property prediction and mixture optimization, notable limitations persist. For instance, Reference [5] pioneered a compact packing model-based approach to UHPC mixture design, achieving 28-day compressive strengths exceeding 135 MPa. Reference [6] employed response surface methodology (RSM) to forecast UHPC mechanical properties, elucidating the influence of fiber content on hardness and flexural strength. Additionally, several studies have developed probabilistic frameworks for UHPC property prediction using experimental datasets. However, these conventional approaches often suffer from resource-intensive trial-and-error processes, prolonged development cycles, computational complexity, and suboptimal predictive accuracy, particularly when applied to non-traditional UHPC systems incorporating industrial by-products like CSFA.

Machine learning (ML) constitutes a computational intelligence paradigm that constructs predictive models by systematically extracting input-output mappings from empirical datasets. Recent advancements in UHPC research have leveraged ML techniques for performance forecasting and mixture proportion optimization, yielding promising results. For instance, Reference [7] pioneered a primitive deep neural network (DNN) framework to predict the mechanical (compressive strength) and durability (corrosion resistance) properties of UHPC, elucidating the impact of key parameters such as water-to-cement ratio and superplasticizer dosage. Subsequent studies, including Reference [8], refined this DNN architecture using genetic algorithm-based hyperparameter tuning, thereby enhancing predictive accuracy for both strength and corrosion-related metrics. In parallel, Reference [9] developed a multi-layer perceptron (MLP) model capable of rapidly estimating UHPC compressive strength and corrosion resistance for arbitrary mixtures without experimental validation, demonstrating the scalability of ML-driven approaches. Reference [10] further expanded the ML toolkit by comparing random forest (RF), support vector machine (SVM), and neural network (NN) models for UHPC property prediction, benchmarking their performance against empirical measurements. However, the integration of carbide slag-fly ash (CSFA) composite admixtures into UHPC formulations introduces material system complexity. CSFA components, which function as structural fillers and pozzolanic reactants, fundamentally alter the concrete's microstructure and mechanical behavior. The heterogeneous composition and variable reactivity of CSFA materials necessitate tailored predictive models and optimization strategies, as conventional UHPC methodologies fail to account for their synergistic effects on strength development and corrosion mitigation. Despite the critical need for advanced ML frameworks in CSFA-modified UHPC systems, current research predominantly focuses on traditional UHPC formulations, leaving a significant knowledge gap regarding data-driven design approaches for this emerging class of sustainable cementitious composites.

Given this context, the present study investigates the synergistic effects of carbide slag-fly ash composite admixtures on the mechanical performance (compressive strength) and durability (corrosion resistance) of environmentally sustainable ultra-high-performance concrete (UHPC). To address prediction challenges associated with imbalanced datasets, a novel deep learning architecture is proposed that incorporates a weighted cross-entropy loss function to enhance model robustness in predicting both strength and corrosion-related properties of UHPC. Empirical evaluations demonstrate that the proposed hybrid deep neural

network outperforms conventional machine learning approaches, exhibiting superior predictive accuracy while maintaining interpretability consistent with practical engineering principles. Through systematic parameter optimization of the deep learning ensemble, optimal admixture proportions for carbide slag-fly ash composites in UHPC formulations were identified. The findings of this research provide a data-driven theoretical framework for rational mixture design of advanced cementitious composites.

2 Related works

Different mineral admixtures, also known as auxiliary cementitious materials, have different chemical compositions, reactivity, particle morphology, fineness, etc [11]. Generally speaking, carbide slag fly ash composite materials are usually finely dispersed low calcium materials, rich in elements such as Si and A1, and have different chemical properties from cement. The addition of carbide slag fly ash composite materials will inevitably make the UHPC composite cementitious system more complex.

Calcium carbide slag and fly ash are by-products of the induction arc smelting process in the silicon metal and ferrosilicon alloy industries. At high temperatures, quartz is reduced to silicon while generating silicon vapor. This gas is oxidized and condensed into small spherical particles (with an average particle size of about 0.1um) at low temperatures. These particles are composed of amorphous silica (>85%) and have high volcanic ash activity. Powdered carbide slag and fly ash can be obtained through dust collection devices. The carbide slag and fly ash are shown in Figure 1.

Figure 1: Calcium carbide slag fly ash

Without considering the workability of the mixture, the effects of carbide slag and fly ash on cement hydration, microstructure evolution, and strength development in UHPC are mainly divided into physical and chemical effects [12].

(1) Physical effect - filler effect. The filling effect is caused by the physical presence of

powder particles, which leads to changes in the hydration process and microstructure of cement. In fact, it includes the following aspects: 1) dilution effect: due to the substitution of some cement by carbide slag and fly ash, the effective water cement ratio is increased under the same water to solid ratio, allowing more water to participate in cement hydration and providing more space for the growth of hydration products; 2) Nucleation effect: Smaller particles, due to their larger specific surface area, can provide nucleation sites for cement hydration products, promoting cement hydration. 3) Accumulation effect: Due to the extremely small particles of carbide slag and fly ash, they can replace water in smaller spaces in concrete, making it denser.

It is worth mentioning that the mechanism explanations for the filling effect in the literature are similar. This article summarizes them into the three aspects mentioned above. The physical effects, nucleation effects, and stacking effects referred to below all refer to the filling effect, which is different from volcanic ash reactions.

(2) Chemical reaction - volcanic ash reaction. Generally speaking, carbide slag fly ash composite materials and Portland cement clinker contain the same chemical elements, but their proportions and combinations in the solid phase composition are different. Therefore, as long as CH is available, the carbide slag fly ash composite material will react in concrete and produce similar hydration products, but the proportion and composition of hydration products will significantly change with changes in dosage and other conditions. The volcanic ash reaction of carbide slag fly ash forms C-S-H:

$$S + 1.7CH + 2.3H \rightarrow C_{1.7}SH_4 \quad (1)$$

Hydration is a reaction process in which cement particles come into contact with water, and clinker minerals undergo hydration with water, transforming from an anhydrous state to a hydrated compound bound to water. This process is a very complex process of physics, chemistry, and physical chemical changes. Over the past century, a considerable number of scholars and experts have conducted research in this field and achieved many results and theories. The mixing of carbide slag fly ash, and Portland cement can lead to a more complex cementitious system [13]: (1) The hydration reaction of cement and the volcanic ash reaction of carbide slag and fly ash occur simultaneously, and may affect each other's reaction activity; (2) The presence of carbide slag and fly ash can affect the quantity and types of hydration products formed in the cementitious system, thereby affecting the volume, porosity, and ultimate durability of the system; (3) The volcanic ash reaction kinetics of carbide slag fly ash depend on its chemical composition, fineness, glass phase content, and pore solution composition. Due to the difficulty in quantitatively analyzing the reaction degree of carbide slag fly ash in complex cementitious systems, little is known about the specific effects of these parameters. Based on the above reasons, the following article summarizes the effects of carbide slag and fly ash on the hydration kinetics and microstructure of complex cementitious systems, attempting to determine the basic principles based on cement chemistry and thermodynamics.

The reactivity of carbide slag and fly ash is highly dependent on the alkalinity and pH value of the pore solution, and the required alkaline environment is formed within the first few days. Therefore, the reaction amount of carbide slag and fly ash before and after the first day of hydration can be ignored. Therefore, the cement hydration kinetics is mainly affected by the filler effect. The influence of filler effect on hydration kinetics is mainly related to the fineness and substitution rate of carbide slag fly ash composite materials [14]. After replacing some cement with carbide slag fly ash composite material, it provides more abundant free water and precipitation space for cement hydration products. The higher the substitution rate, the higher the actual water cement ratio, and the probability of nucleation will also increase with the increase of the number of powder particles. In addition, the smaller the particle size of carbide

slag fly ash composite materials, the larger the specific surface area of the particles, and the more nucleation sites provided. The affinity of the particle surface of carbide slag fly ash composite material for cement hydration products also affects the nucleation effect [15]. Reference [16] indicates that the filler effect cannot be simply explained by providing additional nucleation surfaces, and particle spacing can also affect this effect. The spacing between particles affects the shear force between them, and the smaller the spacing, the greater the shear force between particles. During the mixing process of the mixture, the shear effect of the particles disrupts the double electron layer formed by the dissolved ions around the cement particles, accelerating the migration of ions within the solubility gradient and enabling better dispersion. This also helps the C-S-H micro nuclei formed during the stirring process to move to the particle surface or pores.

The hydration-modulating effects of carbide slag and fly ash on early-stage cement hydration exhibit a dichotomous nature [17]. First, these industrial by-products accelerate hydration kinetics through: (1) a synergistic filling-nucleation mechanism, wherein the fine particles of carbide slag-fly ash composites serve as heterogeneous nucleation sites and create additional precipitation space for cement hydrates, thereby enhancing early-stage hydration rates; (2) preferential adsorption of polycarboxylate ether (PCE) superplasticizer molecules onto the surface of carbide slag and fly ash particles, which mitigates the retarding effects of water-reducing agents by reducing their availability to disrupt cement flocculation. Conversely, carbide slag and fly ash exhibit hydration-inhibiting behaviors via: (1) surface adsorption onto cement grains, which restricts water accessibility to reactive cement phases; (2) particle agglomeration at elevated substitution levels, driven by the high surface energy of these materials, leading to reduced hydration efficiency; (3) competitive adsorption of PCE molecules, which diminishes the dispersive efficacy of superplasticizers and preserves cement flocculation structures to a greater extent [18, 19]. These opposing effects underscore the complexity of carbide slag-fly ash interactions during cement hydration, with the predominant mechanism being system-dependent and evolving dynamically across hydration stages.

3 Data sources and processing

3.1 Data sources

Based on experience, it is speculated that 11 parameters, including water cement ratio (W/B), carbide slag fly ash, cement (SF/C), fly ash, cement (FA/C), quartz acid, cement (S/C), quartz powder, cement (Qu/C), steel fiber content (S-F), PP fiber content (PP-F), hot water curing (HW), dry heat curing (DA), and heating temperature (T), have a strong impact on the residual compressive strength and corrosion resistance of UHPC [20]. For this purpose, this article collected experimental data from relevant literature both domestically and internationally, forming a sample dataset of 226 groups.

3.2 Data Preprocessing

Due to the large number of input variables in the established prediction model, in order to verify the reliability of the sample data, it is necessary to conduct multicollinearity tests between the input variables and eliminate factors with high correlation. This article uses Spearman correlation coefficient method for testing. It is generally believed that when the absolute value of the correlation coefficient between two input variables is ≥ 0.8, there is a certain degree of collinearity between the two variables.

To ensure the objectivity of the evaluation and the scientificity of the input variables in the

selected sample dataset, this paper uses principal component analysis weighting method to assign weights to 11 input variables. After principal component analysis, the contribution rates of 11 principal components were obtained, as shown in Figure 2. When the cumulative contribution rate reaches 80% to 90%, it can be considered that the amount of data information can be basically guaranteed.

According to Figure 2, the number of principal components determined based on cumulative contribution rate in this article is 6, and the cumulative variance contribution rate of the first 6 items is 85.96%, which can basically represent the information of all 11 input variables. The variance contribution rates of the first six principal components after correction are 24.45%, 20.35%, 14.30%, 10.69%, 8.78%, 7.39%, respectively.

In order to train the model more conveniently and scientifically, while eliminating the influence of variable distribution in the sample dataset, the randperm function provided by Matlab software was used to randomly select 172 out of 214 sets of experimental data as the training set and the remaining 42 sets as the testing set.

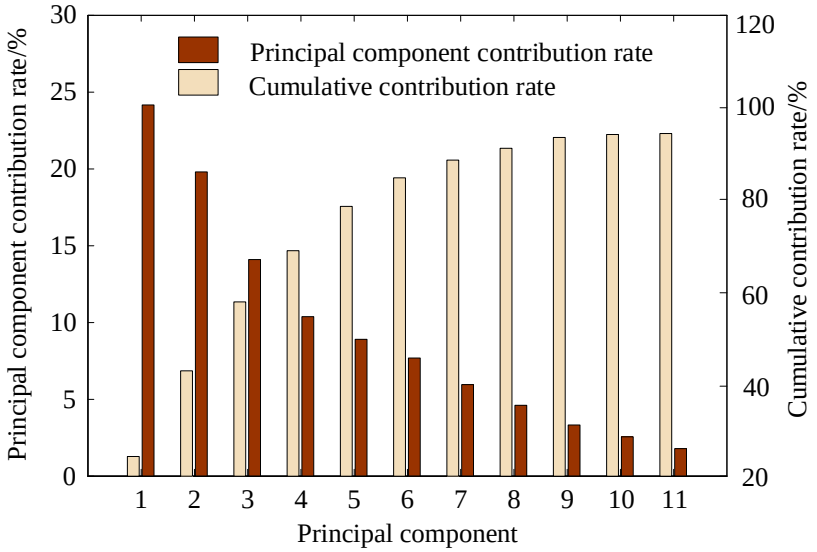

Figure 2: Principal Component Contribution Diagram

3.3 Model evaluation indicators

Because the fitness function used in the improved deep neural network used in this article is the mean square error, the optimal hidden layer node is selected, and the correlation coefficient R^2 and mean square error MSE are used to evaluate the fitting of the model under different hidden layer nodes. The calculation formulas are shown in equations (2) and (3).

$$R = \frac{\sum_{i}^{n}\left[\left(y_i^* - \bar{y}^*\right)\left(y_i - \bar{y}\right)\right]}{\sqrt{\sum_{i}^{n}\left(y_i^* - \bar{y}^*\right)^2 \sum_{i}^{n}\left(y_i - \bar{y}\right)^2}} \tag{2}$$

$$MSE = \frac{1}{n}\sum_{i=1}^{n}\left(y_i^* - y_i\right)^2 \tag{3}$$

where, n is the number of samples; y_i^* and $\bar{y}^*$ are the predicted and average values of the model, respectively; y_i and $\bar{y}$ are the sample experimental values and mean values,

respectively.

To evaluate the predictive performance of the model, three evaluation metrics are introduced: root mean square error (RMSE), mean absolute error (MAE), and coefficient of determination (R^2). The calculation methods are shown in equations (4) to (6).

$$RMSE = \sqrt{\frac{1}{n}\sum_{i=1}^{n}\left(y_i^* - y_i\right)^2} \tag{4}$$

$$MAE = \frac{1}{n}\sum_{i=1}^{n}\left|y_i^* - y_i\right| \tag{5}$$

$$R^2 = 1 - \sum_{i}^{n}\left[\left(y_i^* - y_i\right)^2 \Big/ \sum_{i}^{n}\left(\bar{y} - y_i\right)^2\right] \tag{6}$$

When RMSE and MAE are closer to 0 and R^2 is closer to 1, it indicates that the model's predicted value is closer to the experimental value and the model's prediction accuracy is higher.

4 Improved deep neural network algorithms

This article's method includes two parts: label learning and contrastive learning (Figure 3). In the label learning section, weighted cross entropy loss is introduced to reduce the impact of class imbalance on the model. In the comparative learning section, design supervised comparative learning to enhance the feature extraction capability of the model.

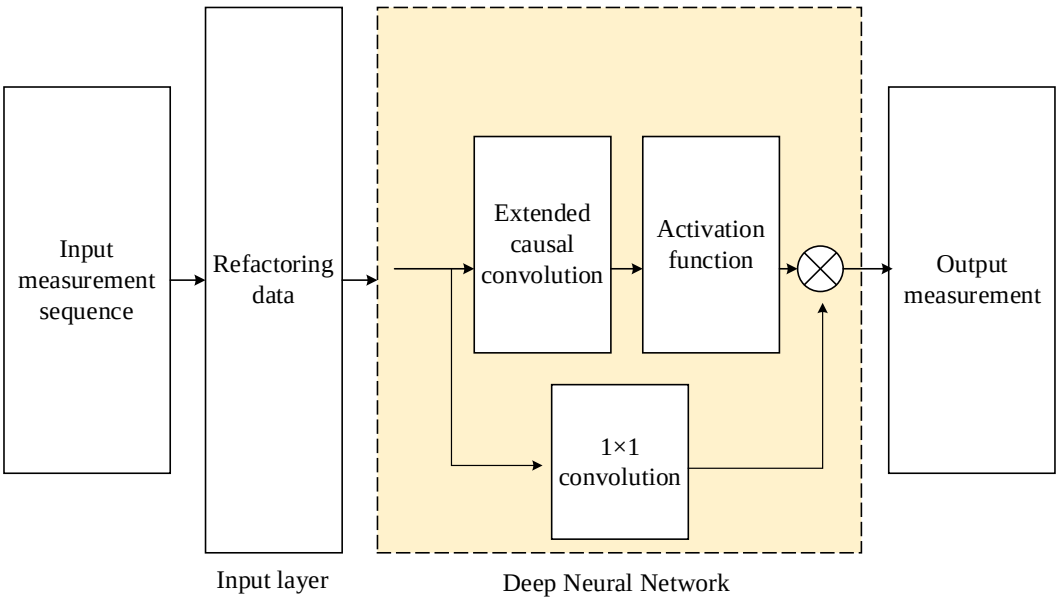

Figure 3: Algorithm Block Diagram

4.1 Model Structure

MLP is a classic feedforward artificial neural network model [21], consisting of an input layer, a hidden layer, and an output layer. Each neuron in the hidden and output layers is connected to all neurons in the previous layer, hence it is also known as a Fully Connected layer (FC). Among them, the hidden layer is responsible for performing a series of nonlinear transformations on the input data to achieve feature extraction, and the output layer is responsible for predicting

sample categories based on the feature embeddings extracted by the hidden layer. This article adopts a two-layer network structure MLP as the prediction model, and embeds the features output by the first layer into AA and the prediction probability matrix BB output by the second layer as follows:

$$\boldsymbol{H} = \boldsymbol{W}^{(1)}\boldsymbol{X} + \boldsymbol{b}^{(1)} \tag{7}$$

$$\boldsymbol{P} = \mathrm{softmax}\left[\sigma\left(\boldsymbol{W}^{(2)}\boldsymbol{H} + \boldsymbol{b}^{(2)}\right)\right] \tag{8}$$

where, $\boldsymbol{W}^{(i)}$ and $\boldsymbol{b}^{(i)}$ represent the trainable parameters of the *i*-th layer, while σ represents the activation function (such as ReLU, Sigmoid, etc.).

Cross entropy loss is one of the commonly used loss functions in classification tasks, and its effectiveness has been widely verified in practice. This article expresses the cross entropy loss function as follows [22, 23]:

$$L_{ce} = -\sum_{i \in T} y_i \log p_i \tag{9}$$

where, $T = v_1, v_2, \cdots, v_t$ represents the training dataset; *t* represents the total number of training samples. y_i and p_i respectively represent the label of sample v_i and the predicted probability distribution of the model for sample v_i. Cross entropy loss can measure the difference between the probability distribution output by the model and the true label. When the difference between the two is large, the value of cross entropy loss will be larger, and vice versa. Therefore, by minimizing the cross-entropy loss, the model can gain the ability to distinguish between different categories. However, when there is a significant difference in the number of samples from different categories in the dataset, using cross entropy loss may cause the model to focus more on the more numerous categories during training and ignore the fewer categories, as traditional cross entropy loss treats all samples fairly.

To address the aforementioned issues, some improvements have been made to equation (9), enabling it to provide varying degrees of attention to samples of different categories. Specifically, a sample reweighting strategy is introduced to assign higher weights to categories with fewer samples, while the opposite is true for categories with more samples. To do this, first calculate the number of samples for each category in the training set:

$$M_i = \sum_{j=1}^{t} 1\left(y_j = i\right) \tag{10}$$

where, M_i represents the number of samples for category *i*; $1(*)$ represents the indicator function, and when the condition in parentheses holds, $1(*) = 1$, otherwise $1(*) = 0$. After calculating the number of samples for each category, calculate the weight of each category's samples in training according to equation (11):

$$w_i = 1 - M_{y_i} / t \tag{11}$$

where, w_i represents the weight of sample BB, where M_{y_i} represents the number of samples with the same category as the node v_i. According to equation (11), the weight of a sample will be inversely proportional to the proportion of its class to the total number of samples. Finally, by combining equations (9) and (11), the weighted cross entropy loss L_{wce} is obtained:

$$L_{\text{wce}} = -\sum_{i \in T} w_i \cdot \left(y_i \log p_i \right) \tag{12}$$

Equation (6) assigns different weights to samples of different categories, allowing the model to learn fairly for each category during training, thereby reducing the impact of class imbalance on model training and achieving better generalization ability.

4.2 Supervision and comparison of losses

Weighted cross entropy loss can enable the model to learn category information from sample labels by minimizing the difference between the predicted results of the model and the true labels [24, 25]. However, it lacks the ability to learn the interrelationships between samples, which often helps the model better capture the intrinsic structure and correlations of data, thereby obtaining higher quality feature embeddings. Based on the above considerations, this article designs a supervised contrastive loss to enable the model to better learn the interrelationships between samples. Specifically, select *i* positive samples and *j* negative samples for each sample, and make them closer to each other in the embedding space and farther away from each other in the embedding space.

(1) Select positive sample. In order to enable the model to learn the connections between samples of the same class, select the part of the sample with the same category and most similar features as its positive sample for each sample, and make them close to each other in the embedding space. Specifically, first divide the training set into multiple subsets according to different categories:

$$\mathrm{C}_i = \left\{ v_j \left| \forall j \in (1, n), y_j = i \right. \right\} \tag{13}$$

where, C_i represents a set composed of samples of category *i*. Next, calculate the feature similarity between each sample and other similar sample:

$$P_i = \left\{ S_{ij} \left| \forall v_j \in C_{y_i} \right. \right\} \tag{14}$$

where, P_i represents the set of similarity between sample v_i and other similar samples, $S_{ij} = x_i \cdot x_j / |x_i||x_j|$ represents the similarity between node v_i and v_j, x_i and x_j represent the feature vectors of nodes v_i and v_j, respectively. Finally, for each sample, select the same type of sample with the highest similarity as its positive sample:

$$Pos_i = top(P_i, k) \tag{15}$$

where, Pos_i represents the set of positive samples selected for sample v_i, while $top(P_i, k)$ represents selecting the top *k* samples with the highest values from P_i. By reducing the distance between samples and their positive samples in the embedding space, the model can better learn the connections between similar samples, thereby improving the feature extraction ability of the model.

(2) Select negative samples. While allowing the model to learn the connections between similar samples, it is also necessary to learn the differences between samples of different categories. Therefore, this article will select the same number of negative samples as the positive samples for each sample. Firstly, calculate the feature similarity between each sample and non-similar samples:

$$N_i = \left\{ S_{ij} \middle| \forall v_j \notin C_{y_i} \right\} \tag{16}$$

where, N_i represents a set of similarities between sample v_i and non-similar samples. Next, in order to enhance the model's ability to distinguish non similar samples with similar features while maintaining its ability to distinguish samples with dissimilar features. Select *k*-1 non similar samples with the highest similarity and one non similar sample with the lowest similarity for each sample as negative samples:

$$Neg_i = top(N_i, k-1) + top(N_i, -1) \tag{17}$$

where, Neg_i represents the set of negative samples selected for sample v_i, $top(N_i, k-1)$ represents selecting the top *k*-1 samples with the highest similarity from N_i, and $top(N_i, -1)$ represents selecting the sample with the lowest similarity from N_i. By increasing the distance between samples and their negative samples in the embedding space, the model can better capture the differences between samples of different categories, resulting in better separation of samples of different categories in the embedding space, thereby improving the classification performance of the model.

5 Experimental analyses

5.1 Improving the Training of Deep Neural Networks

This article uses Matlab software to implement improved deep neural network training for predicting the compressive strength and corrosion resistance of UHPC. The main training process is as follows:

(1) Establishing an improved deep neural network for predicting the compressive strength and corrosion resistance of UHPC. This paper presents a 7-8-1 topology structure,

(2) Select UHPC compressive strength and corrosion resistance prediction improvement deep neural network training samples and take a cross validation fold of *K*=5, which means dividing all data into 5 equal parts, with 4 parts as the training set and 1 part as the testing set

(3) The commonly used algorithm for normalizing training samples of improved deep neural network for predicting compressive strength and corrosion resistance of UHPC is:

$$Y = \frac{X - X_{\min}}{X_{\max} - X_{\min}} \tag{18}$$

where, *Y* is the normalized result, with a range of (0,1); *X* is the training sample; $X_{\min}$ and $X_{\max}$ are the minimum and maximum values in the sample, respectively. The Mapminmax function can also be directly called in Matlab,

(5) Improved deep neural network initial weight and threshold assignment for predicting compressive strength and corrosion resistance of UHPC. When the deep neural network algorithm reaches the maximum learning generation (set as 20 in this paper) or the set indicators, the optimized network connection initial weight and initial threshold are obtained.

(6) Improved training of deep neural network for predicting compressive strength and corrosion resistance of UHPC. The optimized weight threshold is used for network training, and the weights and thresholds of the network are adjusted in reverse by calculating the error with the expected value. After meeting the minimum error, the final weights and thresholds are saved to complete the network training.

5.2 Analysis of Prediction Results

Figure 4 shows the prediction results of the original deep neural network and the improved deep neural network. After calculation, it can be concluded that the absolute values of the relative errors between the predicted samples of 10 sets of original deep neural networks and the true values are 3.15%, 7.87%, 1046%, 3.81%, 7.43%, 2.57%, 11.82%, 1513%, 1.40%, and 0.15%, respectively. The average absolute value of the relative error is 6.48%; Except for the slightly larger error of 1513% in group 8, the prediction performance of the remaining samples is good. The absolute relative errors between the predicted samples of the 10 groups of original deep neural network optimized by genetic algorithm and the true values are 31%, 654%, 306%, 248%, 324%, 31%, 48%, 1.12%, 1.36%, and 157%, respectively. The average relative error is only 214%, which is 30% of the error of the original deep neural network algorithm. It can be seen that the improved deep neural network prediction effect is very good.

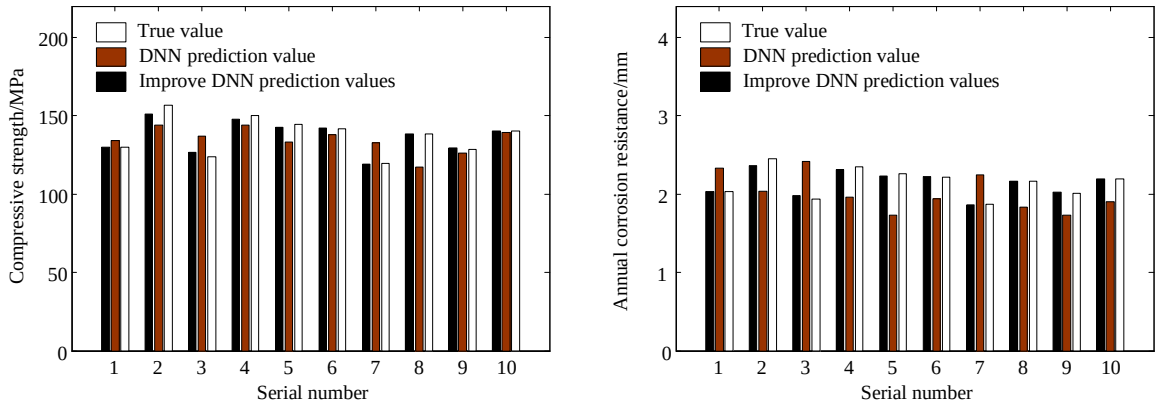

(a) Prediction of compressive strength (b) Corrosion resistance prediction

Figure 4: Prediction Results of Original Deep Neural Network/Improved Deep Neural Network

Figure 5 shows the relative error comparison between the prediction results of the original deep neural network and the improved deep neural network. As shown in Figure 5, the original deep neural network optimized by genetic algorithm has better predictive performance and can better guide the prediction of UHPC compressive strength and corrosion resistance, as well as mix design.

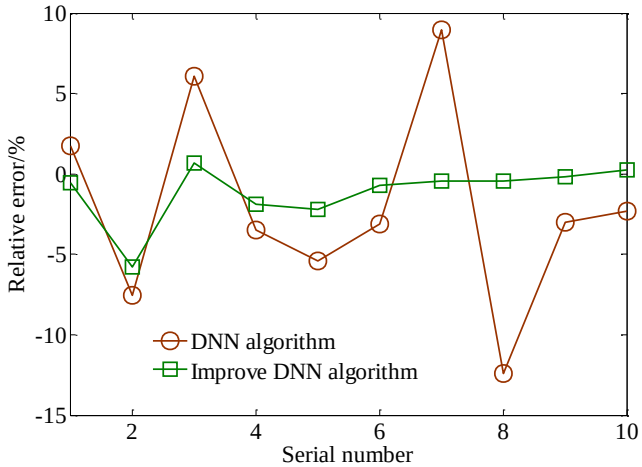

(a) Prediction of compressive strength

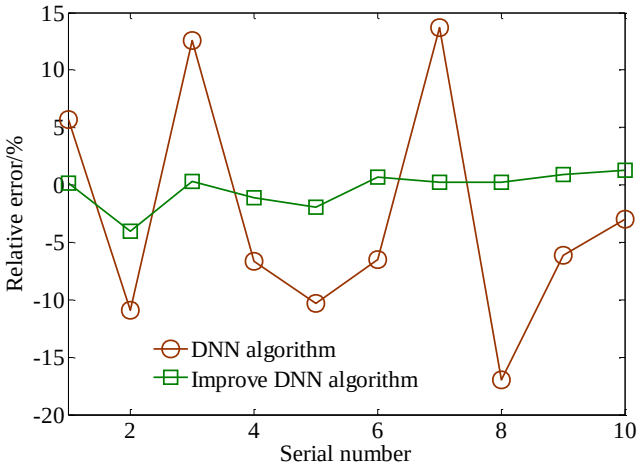

(b) Corrosion resistance prediction

Figure 5: Error Comparison between Original Deep Neural Network and Improved Deep Neural Network

5.3 UHPC mix design method

Applying improved deep neural networks to the optimization design of UHPC mix proportions can not only reduce the waste of human and material resources caused by early trial production, lower production costs, but also incorporate experimental results after each trial, retrain the network, and continuously accumulate knowledge to improve the accuracy and applicability of network prediction. The specific steps are as follows:

(1) Train an improved deep neural network for predicting UHPC performance based on the current mix proportion test sample database.

(2) Adjust the input layer parameters of UHIPC raw materials according to the mix proportion constraints, and predict their corresponding performance parameters through improved deep neural networks.

(3) Establish a correlation between different raw material compositions and performance based on experimental and predictive data.

(4) Design the initial mix proportion of UHPC in reverse based on the correlation established in step (3) with performance indicators as the goal.

(5) Based on engineering requirements and cost control, conduct trial mixing and adjustment of the designed mix proportion, and finally obtain the actual mix proportion for use.

In order to better apply the improved deep neural network prediction model to UHPC mix design, this paper takes the measured values in the data sample and the predicted values of the neural network as examples to analyze the control methods of different factors in UHPC mix design when compressive performance is the target indicator.

Keeping factors such as cement, aggregate, and water cement ratio unchanged, the compressive strength and corrosion resistance of UHPC can be calculated based on the original deep neural network/improved deep neural network under different dosages of carbide slag and fly ash. Taking the 35th to 40th sets of data as an example, using an improved deep neural network can better predict the effect of carbide slag and fly ash. Adding an appropriate amount of carbide slag and fly ash can improve the compactness and mechanical properties of the system, but excessive dosage (exceeding 25%) will have adverse effects on the strength. Under this mix ratio condition, the amount of carbide slag and fly ash in the UHPC mix ratio can be reverse designed based on the predicted curve and the given target performance. For example,

when the target strength is 140MPa, the initial amount of carbide slag and fly ash can be determined to be around 20%, and then the mix ratio design and experimental verification can be carried out.

Based on the 47th to 50th sets of data, it was still found that the improved deep neural network can better predict the effect of steel fibers than the original deep neural network. Moderate amount of steel fiber can significantly improve the compressive strength and corrosion resistance of UHPC, but when its dosage is high, it will have adverse effects on the workability of UHPC. Generally, the comprehensive performance is better when the steel fiber dosage is around 2.0%. Similarly, under this mix ratio condition, the steel fiber content in the UHPC mix ratio can be designed in reverse from the target performance and prediction curve. For example, when the target strength is 140MPa, the steel fiber content in the mix ratio can be preliminarily determined to be around 16.78%, and then the mix ratio design and experimental verification can be carried out.

According to the improved deep neural network model mentioned above, it can be concluded that the compressive strength and corrosion resistance of UHPC are predicted as follows:

(1) From the error distribution graph, it can be seen that the error distribution curve of the model training set conforms to normal distribution characteristics, indicating that the model can accurately analyze the coupling effect of multiple input variables on the compressive strength and corrosion resistance of UHPC during the training process. The prediction error is basically controlled within 14.26%, and the predicted values of the model are close to the experimental values. After learning the training data of UHPC compressive strength and corrosion resistance, the model has good generalization ability and can be used to predict the compressive strength and corrosion resistance of UHPC under multiple factors.

(2) Combining the error distribution map and scatter fitting map, it can be seen that although the original deep neural network model has high prediction accuracy during training, there are individual cases with large dispersion errors.

(3) Compared with the original deep neural network, the root mean square error (RMSE) of the improved and optimized deep neural network model decreased by 17.21% and 41.26% respectively, the average absolute error (MAE) decreased by 28.35% and 44.25% respectively, and the R^2 increased from 0.876 to 0.913 and 0.927, indicating that the improved optimization algorithm significantly improves the predictive performance of the deep neural network and compensates for the shortcomings of the original deep neural network model in global optimization.

(4) Overall, the optimal prediction model is an improved deep neural network model, with an error distribution that approximates a standard normal distribution. Its evaluation metrics RMSE is 7.823, MAE is 6.415, and R2 is 0.936, indicating that the improved deep neural network model has higher robustness compared to other models and is less likely to fall into local optima.

6 Conclusion

(1) The improvement of deep neural network prediction accuracy is mainly affected by parameters such as training algorithm and the number of hidden layer nodes. The improved deep neural network designed in this study has good prediction accuracy for the compressive strength and corrosion resistance of UHPC composite material made of carbide slag, slag and fly ash. Compared to the original deep neural network, the improved deep neural network has higher prediction accuracy and stronger generalization ability.

(2) Based on improved deep neural networks, the mix design of UHPC composite materials

with specific strength grades of carbide slag, slag and fly ash can be adjusted and optimized. Taking into account the compressive strength, corrosion resistance, and preparation cost, it is recommended that the value of the cementitious material for carbide slag fly ash composite materials be between 0 and 0.9; Taking into account compressive strength, corrosion resistance, particle size distribution, and bulk density, it is recommended to set the sand cement ratio between 1.2 and 1.8.

(3) Due to limited data samples and parameter analysis, there is still room for further optimization of the improved deep neural network established in this study. Future research will focus on comprehensively considering multiple factors such as preparation cost, compressive strength and corrosion resistance, tensile strength, and workability to further optimize the mix design of calcium carbide slag fly ash composite material UHPC, as well as using different optimization algorithms, increasing the data sample size, studying more sufficient parameter analysis such as different hidden layer numbers, genetic generations, and variation functions, and further improving the prediction accuracy of the original deep neural network for the compressive strength and corrosion resistance of calcium carbide slag fly ash composite material UHPC, guiding the mix design of calcium carbide slag fly ash composite material UHPC.

About the Author

Haozhe Pan, He was born in Zhenjiang, Jiangsu, China, in 1992. His main research direction is low-carbon Cementitious Material.

Xingpei Yan, He was born in Nanyang, Henan, China, in 1994. Her main research direction is low-carbon Ultra-High-Performance Concrete.

References

[1] Yoo D Y, Banthia N, Yoon Y S. Recent development of innovative steel fibers for ultra-high-performance concrete (UHPC): a critical review[J]. Cement and Concrete Composites, 2024, 145: 105359.

[2] Su X, Ren Z, Li P. Review on physical and chemical activation strategies for ultra-high-performance concrete (UHPC)[J]. Cement and Concrete Composites, 2024: 105519.

[3] Zhang W, Zheng D, Huang Y, et al. Experimental and simulative analysis of flexural performance in UHPC-RC hybrid beams[J]. Construction and Building Materials, 2024, 436: 136889.

[4] Zhang Y X, Zhang Q, Xu L Y, et al. Transfer learning for intelligent design of lightweight strain-hardening ultra-high-performance concrete (SH-UHPC)[J]. Automation in Construction, 2025, 175: 106241.

[5] Fan D, Lu J X, Liu K, et al. Multi-scale design of ultra-high performance concrete (UHPC) composites with centroplasm theory[J]. Composites Part B: Engineering, 2024, 281: 111562.

[6] Wakjira T G, Kutty A A, Alam M S. A novel framework for develo** environmentally sustainable and cost-effective ultra-high-performance concrete (UHPC) using advanced machine learning and multi-objective optimization techniques[J]. Construction and

Building Materials, 2024, 416: 135114.

[7] Zhao L, Luo Q. Evaluating bonding strength in UHPC-NC composite: A comprehensive review of direct and indirect characterization methods[J]. Construction and Building Materials, 2024, 443: 137701.

[8] Shah H A, Du J, Meng W. Low-carbon UHPC with carbonated blast furnace slag: Impact of mineral composition, carbonation degree, and CaCO3 polymorphs[J]. Cement and Concrete Composites, 2025, 160: 106039.

[9] Fang Z, Wu J, Xu X, et al. Grouped rubber-sleeved studs–UHPC pocket connections in prefabricated steel–UHPC composite beams: Shear performance under monotonic and cyclic loadings[J]. Engineering Structures, 2024, 305: 117781.

[10] Silva M L, Prado L P, Félix E F, et al. The influence of materials on the mechanical properties of ultra-high-performance concrete (UHPC): a literature review[J]. Materials, 2024, 17(8): 1801.

[11] Li Y, Zhou H, Zhang Z, et al. Macro-micro investigation on the coefficient of friction on the interface between steel and cast-in-place UHPC[J]. Engineering Structures, 2024, 318: 118769.

[12] Feng J, Shao X, Qiu M, et al. Reliability evaluation of flexural capacity design provision for UHPC beams reinforced with steel rebars/prestressing tendons[J]. Engineering Structures, 2024, 300: 117160.

[13] Lin J X, Luo R H, Su J Y, et al. Coarse synthetic fibers (PP and POM) as a replacement to steel fibers in UHPC: Tensile behavior, environmental and economic assessment[J]. Construction and Building Materials, 2024, 412: 134654.

[14] Zhang W, Lin J, Huang Y, et al. Temperature-dependent debonding behavior of adhesively bonded CFRP-UHPC interface[J]. Composite Structures, 2024, 340: 118200.

[15] Kravanja G, Mumtaz A R, Kravanja S. A comprehensive review of the advances, manufacturing, properties, innovations, environmental impact and applications of Ultra-High-Performance Concrete (UHPC)[J]. Buildings, 2024, 14(2): 382.

[16] Das P, Kashem A. Hybrid machine learning approach to prediction of the compressive and flexural strengths of UHPC and parametric analysis with shapley additive explanations[J]. Case Studies in Construction Materials, 2024, 20: e02723.

[17] Katlav M, Ergen F. Improved forecasting of the compressive strength of ultra-high-performance concrete (UHPC) via the CatBoost model optimized with different algorithms[J]. Structural Concrete, 2025, 26(1): 212-235.

[18] Xu L, Fan D, Liu K, et al. A machine learning framework for intelligent development of Ultra-High performance concrete (UHPC): From dataset cleaning to performance predicting[J]. Expert Systems with Applications, 2024, 242: 122790.

[19] Ghahsareh F M, Zhang Q, Poorghasem S, et al. Cradle-to-grave life-cycle assessment of ultra-high-performance concrete (UHPC) beams based on real-time monitoring data[J].

Journal of Cleaner Production, 2025, 495: 145098.

[20] Ye M, Li L, Pei B, et al. A critical review on shear performance of joints in precast Ultra-High-Performance Concrete (UHPC) segmental bridges[J]. Engineering Structures, 2024, 301: 117224.

[21] Mikriukov G, Schwalbe G, Bade K. Local Concept Embeddings for Analysis of Concept Distributions in Vision DNN Feature Spaces[J]. International Journal of Computer Vision, 2025: 1-51.

[22] Hayat M, Raza A, Akbar S, et al. pACPs-DNN: Predicting anticancer peptides using novel peptide transformation into evolutionary and structure matrix-based images with self-attention deep learning model[J]. Computational Biology and Chemistry, 2025, 117: 108441.

[23] Li C, Liu S, Jiang K, et al. DNN Inference Acceleration Based on Adaptive Task Partitioning and Offloading in Embedded VEC[J]. ACM Transactions on Embedded Computing Systems, 2025, 24(4): 1-35.

[24] Cao L, Pan H, Li X, et al. Predicting optimal primary tuning parameters of PTTMDI for vortex-induced vibration control of super-tall buildings using physics information enhanced DNN[J]. Engineering Structures, 2025, 334: 120268.

[25] Selvan C, Anwar B H, Naveen S, et al. Ambulance route optimization in a mobile ambulance dispatch system using deep neural network (DNN)[J]. Scientific Reports, 2025, 15(1): 14232.